Supplementary Information:

Table S1: GLMM models of seed:ovule ratio, specialization (d'), and disturbance, and the interaction between d' and disturbance, with the full model (disturbance) against models with the predictors disturbance, d', or the interaction between disturbance and d' dropped from the model (dropdisturbance, dropd, disturbance_add, respectively). All models included species identity and species nested within quadrats and sites as a random effect.

	K	AICc	ΔAICc	AICcWt	Cum.Wt	LL
disturbance (full)	9	14842.96	0	0.98	0.98	-7412.45
dropdisturbance	7	14852.02	9.06	0.01	0.99	-7418.99
dropd	7	14853.32	10.36	0.01	1	-7419.64
disturbance_add	8	14853.95	11	0	1	-7418.95

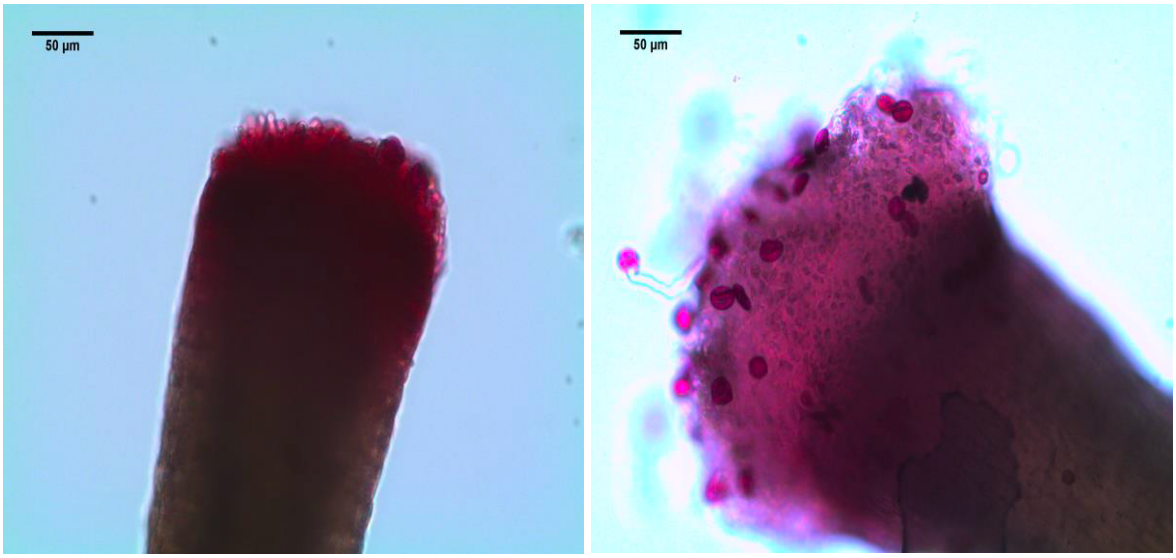

Figure S1: Representative stigmas stained in a few drops of 1% basic fuchsin for a few seconds, rinsed with water and mounted on glass slides with coverslips in 50% glycerin

Left panel features a broken stigma in the outcross group at 200X magnification in which only the most basal part is still left intact. Right panel features a stigma in the control group at 200X magnification with pollen grains visible.

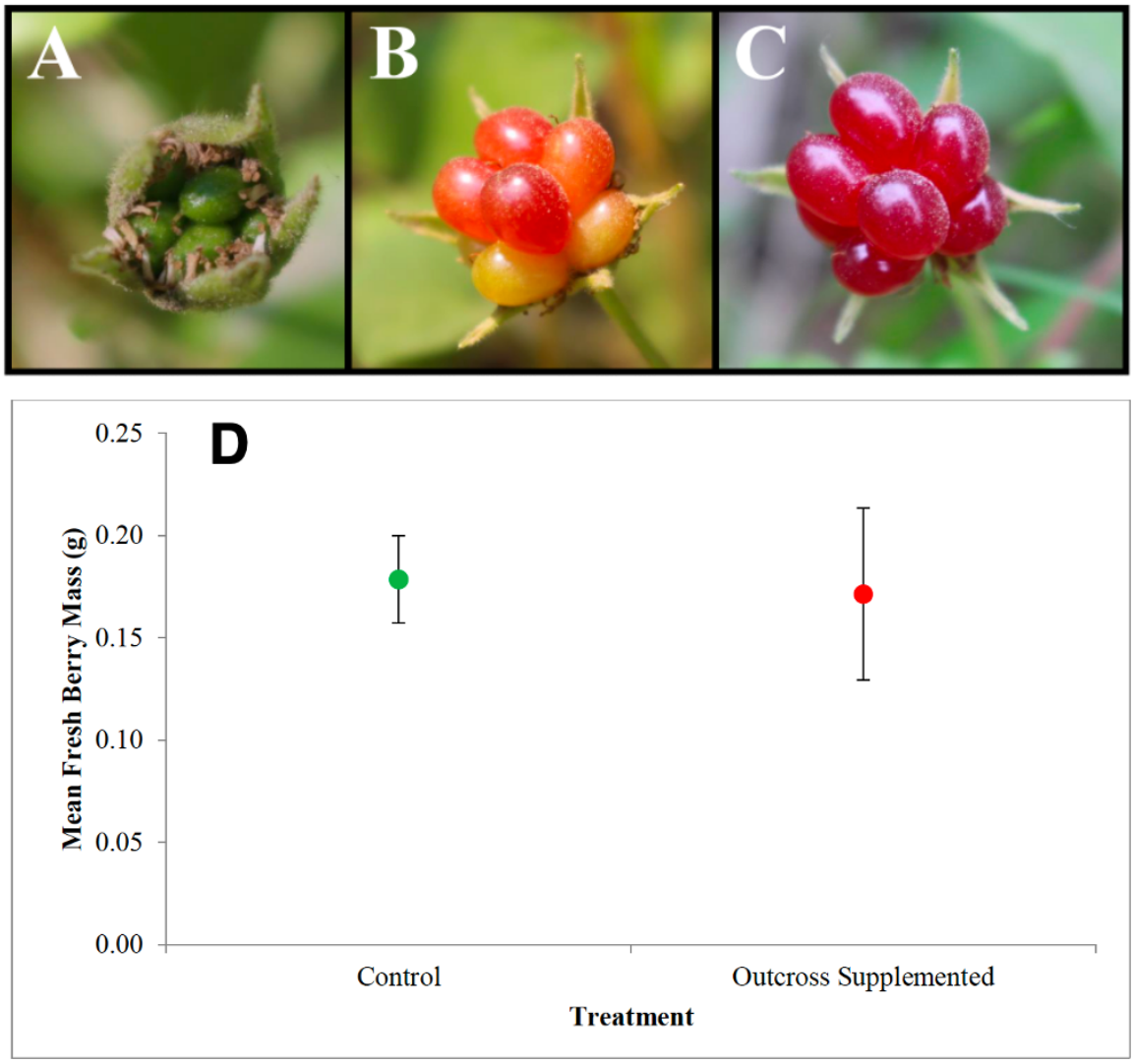

Figure S2: The fruit development, ripening stages, and berry mass of a *Rubus arcticus* spp. *arcticus* berry. A. three weeks post ovule fertilization/three weeks prior to harvesting (note number of pistils not developing); B. < six weeks post ovule fertilization/three days prior to harvesting; C. six weeks post ovule fertilization/day of harvesting. The time span of these images was from June 27th – July 20th, 2017; D. The mean fresh berry bass (g) for the control (N=14) and outcross supplemented (N=7) treatment groups for the pollination supplementation experiment. The mean berry mass includes the collective mass for all the drupelets as well as the receptacle when freshly harvested in the field. Error bars represent standard error.

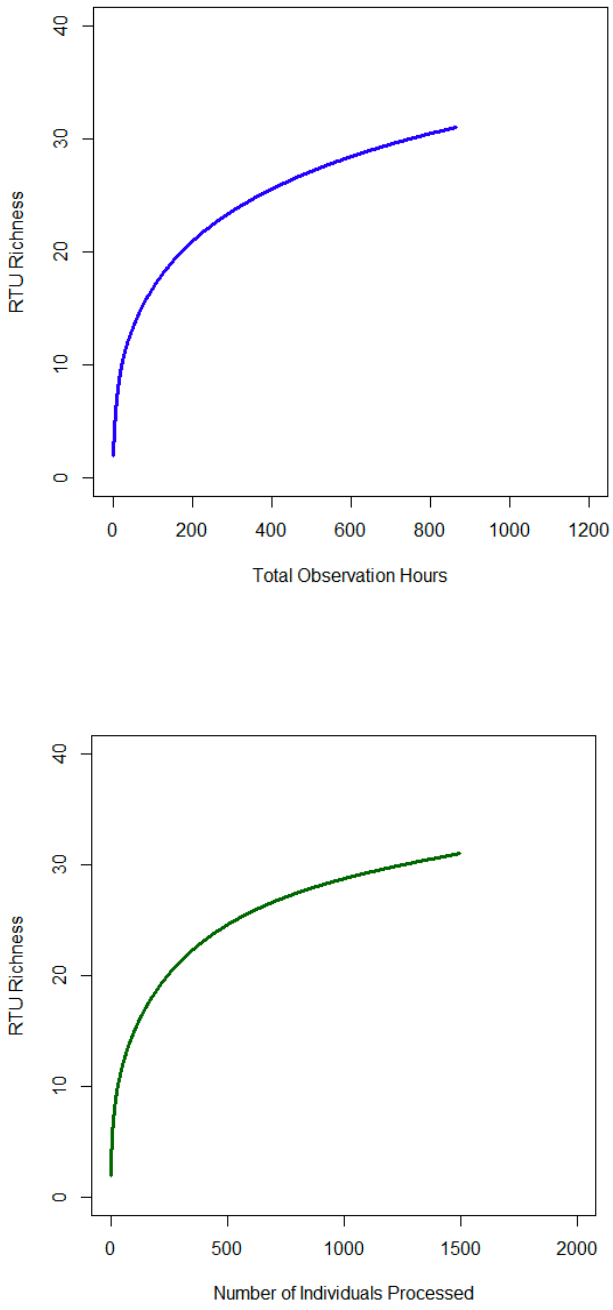

Figure S3: Species accumulation curves with daily Recognizable Taxonomic Unit (RTU) richness as a function of sampling effort. The upper panel has the sampling effort as total observation hours recorded by the time-lapse cameras whereas the lower panel is effort by the number of insects processed or observed visiting focal *R. arcticus* flowers.

Table S2: GLMM models of pollen quantity, pollination treatment (control, outcrossed pollen applied, selfed pollen applied), and observations of stigma breakage, ranked by support. All models included flower as a random effect.

	K	AICc	ΔAICc	AICcWt	Cum.Wt	Res.LL
Treatment: Stigma breakage	8	1485.45	0	1	1	-734.52
Treatment + Stigma breakage	6	1504.92	19.47	0	1	-746.34
Stigma Breakage	4	1506.05	20.6	0	1	-748.97
Treatment	5	1529.12	43.67	0	1	-759.47

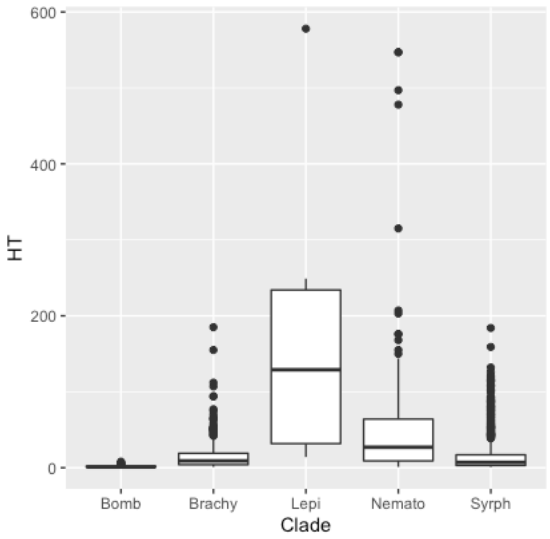

Figure S4: Differences in handling times (HT; measured in seconds) between the main clades of visitors, with skew revealing tendencies of different groups to idle on flowers. In the main models (see Table 2), pairwise differences between groups were significant according to Tukey's HSD test at $p < 0.05$. Bomb = *Bombus* (bumblebees); Brachy = brachyceran flies; Lepi = Lepidopterans; Nemato = Nematocera (mosquitoes); Syrph = Syrphidae.

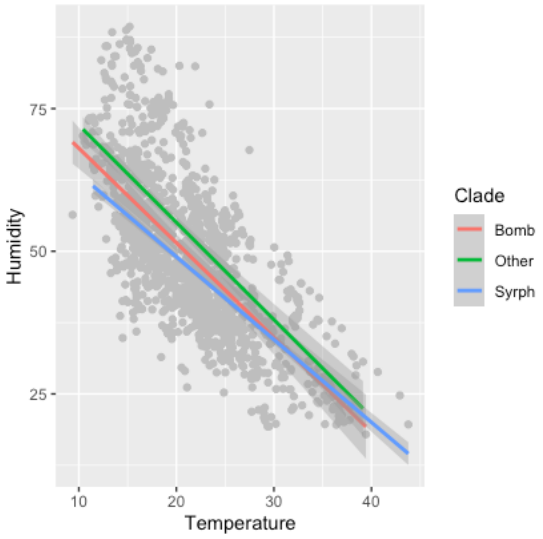

Figure S5: Responses of main visiting clades (*Bombus*, or bumblebees, and Syrphids, with other visitors categorized as "other") to the two main abiotic predictors. Syrphids tended to visit in periods of higher temperatures and lower humidity than other clades.

Supplementary Appendix: GLA Configuration Settings and Methods

The first step in using GLA is registering the hemispherical image. This process involves manually overlaying the photo with a reference circle which defines the actual portions of the photo from the non-required black background (Figure SA1). Each image had a unique registration as some photos varied in size due to some very slight zoom differences, but the initial cursor point was always placed at the top centre of hemispherical photo. After registering a hemispherical image, GLA requires additional "Configuration Settings" which can be divided into four different categories: image, site, resolution, and radiation. For the "Image" tab, all reference hemispherical images had the "registration" set with the initial cursor point at north along with the top of the image being "Geographic North" and the "Projection Distortion" set to "Orthographic". In the "Site" tab; the latitude, longitude, elevation, aspect and slope input were set to the corresponding values for respective focal flower position. Within the "Resolution" tab, solar time step was set to 1 minute and the growing season start date and end date were both set to the corresponding observation day's date, which allows GLA to compute the total radiation received for just that day only (Frazer et al. 1999). The finest temporal resolution GLA can compute to is one day, but Zorer et al. (2013) managed to create hourly simulations within the program. However, they did this with the assistance of a pyranometer coupled with their hemispherical reference photographs. The "Number of Azimuth Regions" was set to 48 and "Number of Zenith Regions" set to 12 as done in Zorer et al (2013). In the "Radiation" tab and for the "Sky Region Brightness" settings, the clear sky coefficient was kept at 0.65 since in North America, this value falls somewhere between 0.6 – 0.7 (Frazer et al. 1999). And lastly, the default Universal Overcast Sky Model (UOC), which assumes all sky regions to be equally bright, was left unchanged.

The “Radiation” tab also has a series of “Model Parameters”. Solar constant was always kept at the default 1367 W/m^2 as recommended by Frazer et al (1999) and units were set to mols/m^2/d. However, cloudiness index (Kt), spectral fraction (R_p/R_s) and beam fraction (Hb/H) are all regional specific parameters had to be calculated separately for each observation day and could not remain constant. Kt is a measure of cloudiness for a given site and the following equation (Lui and Jordan 1960, Iqbal 1983) was used to compute it:

$Kt = H/H_0$

H = Global radiation incident on the ground

H_0 = Extraterrestrial radiation incident on a horizontal surface outside

H can be data from regional solar radiation measurements, thus solar radiation data from the climate data set from the Barrier Lake Research Station (F. Lodhawalla, Personal Communication, September 10, 2017) was used as reference for this variable. H_0 was computed by using GLA’s “Compute Extraterrestrial Radiation” tool in the “Utilities Menu”. Both variables have to be for the same time period and same units (Frazer et al. 1999). Since the data from the Barrier Lake Research Station was in W/m^2, H_0 was also computed in W/m^2. Lastly, to have the H in the same temporal resolution as H_0, the solar radiation was averaged across all 24 hourly measurements from the Barrier Lake Research Station’s pyranometer to produce a daily average for a given observation day.

Spectral fraction is simply the ratio of photosynthetically active radiation (PAR) or visible light in the spectrum of 400-700nm (R_p) to the total shortwave radiation (R_s) contributed by all wavelengths (0.25 μm to 25 μm). This ratio can be directly collected by having a pyranometer paired with quantum sensor to measure PAR, side by side (Frazer et al. 1999).

However, no regional PAR data was available for use and instead, the following equation was used to predict the ratio:

$$\frac{R_p}{R_s} = 1 - \exp\left(-.499Kt^{-0.219}\right)$$

Beam fraction is a ratio of direct (beam) radiation energy (H_b) to total radiation global radiation incident on the ground. The portions of radiation that is scattered by the earth's atmosphere is diffuse radiation whereas the portion that reaches the earth's surface uniformly is direct radiation. Similar to spectral fraction, an equation was used to predict beam fraction. Numerous functions have been created which allow Kt to separate H_b from H (Iqbal 1983, Spitters et al. 1986), which ultimately resulted in the conception of the Atmospheric Environment Service algorithm (Frazer et al. 1999). This algorithm is as follows:

$$\frac{H_b}{H} = \left[1 - \exp\left(-3.044Kt^{2.436}\right]\right.$$

After all the configuration settings had been specified for each registered reference hemispherical image, the blue colour channel was selected within the "Choose A Colour Pane" tool. As recommended by several authors (Lee et al 1983; Frazer et al. 1999, 2001; Nobis and Hunziker 2005, Zorer et al. 2013), this colour best separates the canopy from the sky (Figure S3A. The working images were then transformed into binary images (Figure S3B) using the "Threshold" tool. The threshold value was manually adjusted in every reference image to include as much of the actual canopy vegetation as possible to accurately compute the solar radiation. In the few cases when the sun was visible through the canopy creating the "pinhole effect", GLA's "Draw" tool was used to manually fill in these gaps as accurately as possible. Following the thresholding of the reference image, the "Calculate" function was run with "Canopy Structure and Transmitted Gap Light" selected. GLA then will provide an output summary log with

numerous results, but only “% Canopy Openness” and “Trans Total” (Total transmitted radiation which is the sum of direct and diffuse radiation) were recorded.

Literature Cited

Frazer, G.W., C.D Canham and K.P. Lertzman. 1999. Gap Light Analyzer (GLA), Version 2.0: Imaging software to extract canopy structure and gap light transmission indices from true -colour fisheye photographs, users manual and program documentation. Copyright © 1999: Simon Fraser University, Burnaby, British Columbia, and the Institute of Ecosystem Studies, Millbrook, New York.

Frazer, G.W., R.A. Fournier, J.A. Trofymowc and R.J. Hall. 2001. A comparison of digital and film fisheye photography for analysis of forest canopy structure and gap light transmission. Agriculture and Forest Meteorology 109: 249-263.

Jia, X., R. Huang, Y. Zhou and Z. Su. 2015. Patterns of Understory Plant Diversity in Response to Transmitted Solar Radiation in a Subtropical Forest. International Symposium on Material, Energy and Environment Engineering.

Iqbal, M. 1983. An introduction to solar radiation. Academic Press, Orlando, FL.

Lee, Y.J., R.I. Alfaro and G.A. Van Sickle. 1983. Tree-crown defoliation measurement from digitized photographs. Canadian Journal of Forest Research 13: 956-961.

Lui, B.Y.H., and R.C. Jordan. 1960. The interrelationship and characteristic distribution of direct, diffuse and total solar radiation. Solar Energy 4: 1-19.

Nobis M. and U. Hunziker. 2005. Automatic thresholding for hemispherical canopy-photographs based on edge detection. Agricultural and Forest Meteorology128: 243-250.

Spitters, C.J.T., Toussaint, A.J.M., and Goudriaan, J. 1986. Separating the diffuse and direct component of global radiation and its implications for modeling canopy photosynthesis. Part I. Components of incoming radiation. Agricultural and Forest Meteorology 38: 217-229.

Zorer, R., T. Moffat, A. Strever and J.J. Hunter. 2013. Hourly simulation of grape bunch light microclimate using hemispherical photography. Ciência e Técnica Vitivinícola 28:1031 - 1034.

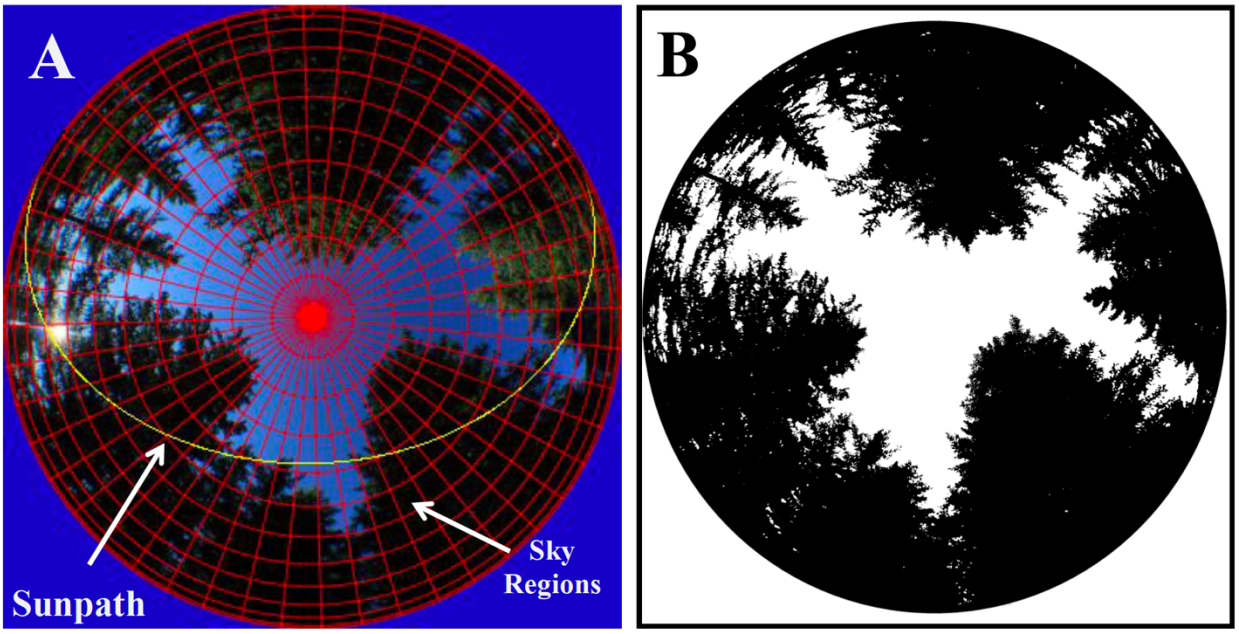

Figure SA1: The GLA simulation process to assess solar radiation exposure. 'A' shows a hemispherical image with the "overlay mask" function (non-usable areas in blue) with the sun path and sky region graticules on top the image. 'B' shows the threshold binary image in which the sky pixels are white and canopy/vegetation pixels